ELSEVIER

Journal of Molecular Catalysis A: Chemical 119 (1997) 425–436

JOURNAL OF MOLECULAR CATALYSIS A: CHEMICAL

Ab initio embedding studies of chemisorption on metal surfaces — interaction of small C–N containing molecules with Ni(111)

Hong Yang *

Department of Chemistry, North Carolina State University, Raleigh, NC 27695-8204, USA

Received 22 June 1996; accepted 23 July 1996

Abstract

This paper briefly describes a theoretical approach for treating chemisorption and surface reactions on metal surfaces. Electronic structures are described by an ab initio configuration interaction embedding theory that allows one to calculate accurately the reaction energetics and adsorption geometries. Adsorption studies of CN, HCN, HNC, CNH_2 and HCNH molecules on Ni(111) are reported. The present calculations show that CN is able to bind to the surface either via the C, or N, or in a side-on geometry with very small differences in total energy (≈ 2 kcal/mol). Adsorption energies at 3-fold, bridge and atop sites are comparable, 113–115 kcal/mol, with the fcc 3-fold site more favorable over other adsorption sites by 2 kcal/mol. Within an energy range of 5 kcal/mol, the CN molecule is free to rotate to other geometries. Both HCN and HNC bind to the surface in an end-on geometry with the molecular axis perpendicular to the surface. The calculated adsorption energy for the end-on HCN is 18, and 11 kcal/mol for the end-on HNC. The side-on bonded HCN and HNC with the C–N bond parallel to the surface are energetically less stable than the corresponding end-on bonded species. Both CNH_2 and HCNH strongly bind to the surface with HCNH more stable by 32 kcal/mol. CNH_2 is adsorbed at a bridge site via the C atom. Both C and N atoms in HCNH are involved in bonding to the surface with the C–N bond parallel to the surface.

Keywords: Ab initio quantum chemical embedded cluster calculations; Chemisorption; Cyanide, hydrogen cyanide, HCNH, CNH_2 and nickel

1. Introduction

First principles ab initio cluster and density functional slab methods have commonly been used to address surface processes, including chemisorption energetics, adsorbate structure and spectra, and heats of reaction and activation energies of surface reactions [1–34]. Both methods are capable of giving high quality solutions. Slab and ab initio cluster calculations each have their special advantages and can provide complementary information. Ab initio cluster calculations tend to model single isolated adsorbed species (or two adsorbed species in the case of coadsorption) in the low surface coverage regime, while slab calculations are better suited to model adsorbate overlayers and the substrate band structure at higher coverages. Slabs have now been employed to investigate surface and interstitial impurities. Recent studies by Head

* Fax: +1-919-5155079; e-mail: hong_yang@ncsu.edu.

PII S1381-1169(96)00506-7

and co-workers showed that slab and ab initio cluster calculations are able to produce comparable results when they both model the adsorbate–substrate interaction under similar conditions [31,32].

In principle, ab initio cluster calculations ought to be the most straightforward method to theoretically study surface processes. There are many examples in which direct cluster models have provided accurate descriptions of adsorption energetics and geometry, vibrational spectra and core level shifts. In practice, one needs to consider the effect of the boundary atoms on the cluster's capability of modeling a surface when a large cluster with a sufficient number of surface atoms is needed to describe surface reactions and coadsorbed species. Thus, the difficulty in treating such topics using the first principles theory is that there are conflicting demands on the theory: at the surface, the treatment must be accurate enough to describe surface–adsorbate bonds and energy changes accompanying molecular reactions, while for a metal, a large number of atoms is required to describe conduction and charge transfer processes.

An alternative approach is to reorganize the theory so as to achieve a description of higher accuracy for the adsorbate and for the metal atoms in the region of the surface near the adsorbate while coupling this cluster to a less accurately described bulk lattice, i.e., to perform embedded cluster calculations. Many different slab and ab initio embedding schemes have been explored [19–34]. The present paper, which is an example of embedded cluster calculations, studies the adsorption of CN, HCN, HNC, CNH_2 and HCNH molecules on Ni(111). The adsorbate and local surface region are embedded in a larger cluster representing the metal lattice. Nickel 3d orbitals are explicitly included on the nickel atoms of the surface region. Our theoretical approach allows us to optimize the geometry of adsorbed CN-containing molecules and to calculate the stability of adsorbates and adsorption energy at various sites on Ni(111).

2. Theoretical approach and calculations

Total energy calculations are performed using a many-electron embedding theory that permits the accurate computation of molecule–solid surface interactions. The present embedding theory is a cluster approach. The objective of the technique is to use ab initio configuration interaction theory to describe surface reactions involving bond formation or dissociation, i.e., to treat interactions at or near the surface adsorption site accurately, while maintaining a coupling to the delocalized lattice electrons. All electron–electron interactions are explicitly calculated and there are no exchange approximations or empirical parameters. Calculations are carried out for the full electrostatic Hamiltonian of the system (except for core electron pseudopotentials), and wavefunctions are constructed by self-consistent-field (SCF) and multi-reference configuration interaction (CI) expansions.

In the present embedding approach, a local surface region is defined as an N-electron subspace extracted from the remainder of the lattice by a localization (electron exchange maximization) transformation. The adsorbate and local region are then treated at high accuracy as embedded in the Coulomb and exchange field of the remainder of the electronic system [33,34]. Coadsorption and surface reaction studies are carried out on the embedded cluster simulating different portions of the metal surface in the presence of a pseudopotential representing the lattice electrons, and the total energy of the cluster plus adsorbate is calculated as a function of the relative position and orientation of the adsorbed species. The approach is summarized below.

We begin to deal with the most delocalized part of the electronic system, the s, p band on a large cluster of atoms (typically 80 to 100); d functions on surface metal atoms are added after a surface s, p electronic subspace is defined. SCF calculations are performed on the s band of the initial cluster and the resulting occupied

orbitals are localized by a unitary transformation based on the maximization of exchange interactions with bulk atomic orbitals. The magnitude of the exchange interaction, γ_k, of a localized orbital, ϕ_k, can be used to determine its degree of localization with respect to the bulk or its penetration into the embedded cluster,

$$\underset{\text{bulk}}{\gamma_1} \geq \gamma_2 \geq \gamma_3 \cdots \gtrsim_{\text{I}} \gamma_m \cdots \geq \underset{\text{surface}}{\gamma_N}$$

where I denotes the boundary of the embedded cluster. For an appropriate choice of m, the localized orbitals, $\phi_1\phi_2 \ldots \phi_m$, primarily reside on atoms in the bulk, but tails extend into the interior of the cluster and toward the surface. The penetrating electron distributions are represented by Coulombic and exchange potentials, $|1/r_{12}\,\rho(2)\rangle$ and $|1/r_{12}\gamma(1,2)\rangle$, and projectors, $\Sigma_m \epsilon_m |Q_m\rangle\langle Q_m|$.

The treatment of the adsorbate–surface system is then carried out by augmenting the basis in the region around the surface sites of interest to include functions describing polarization and correlation contribution. Valence d functions on surface metal atoms are introduced explicitly at this stage. Final electronic wavefunctions including the adsorbate are constructed by configuration interaction,

$$\psi = \Sigma_k \lambda_k \det\left(\chi_1^k \chi_2^k \chi_3^k \cdots \chi_n^k\right)$$

and the coupling of the local electronic subspace and adsorbate to the bulk lattice electrons, $\{\phi_j,\ j = 1,\ m\}$, is represented by the modified Hamiltonian,

$$H = \Sigma_i^N - 1/2\nabla_i^2 + \Sigma_i^N \Sigma_k^Q - Z_k/r_{ki} + \Sigma_{i<j}^N 1/r_{ij} + \Sigma_i^N V_i^{\text{eff}}$$

where

$$\langle a(1)|V_1^{\text{eff}}|b(1)\rangle = \langle a(1)b(1)|1/r_{12}|\,\rho(2)\rangle + \langle a(1)b(1)|1/r_{12}|\gamma(1,2)\rangle + \Sigma_m \epsilon_m \langle a|Q_m\rangle\langle Q_m|b\rangle$$

and ρ, γ, and Q_m denote densities, exchange functions, and atomic orbitals derived from $\{\phi_j,\ j = l,\ m\}$, respectively.

Configuration interaction expansions, ψ, are generated from an initial configuration, or set of configurations, ψ_0, by single and double excitations from the adsorbate–surface region to give excited configurations, ψ_k, and $\psi = c_0\psi_0 + \Sigma c_k \psi_k$.

The N dependency problem with CI expansions is controlled by maintaining a fixed number of electrons in the local subspace and by the multideterminant nature of ψ_0.

Configurations, including the full set of spin permutations, are retained if an interaction threshold,

$$|\langle \psi_k|H|\psi_0\rangle|^2/(E_k - E_0) > \delta$$

is satisfied. Typical CI expansions contain about 3000 to 5000 configurations if the interaction threshold, δ, of 1.0×10^{-6} a.u. is used. Contributions of excluded configurations are determined from extrapolation procedures based on second order perturbation theory.

In most of the applications completed to date, the level of computational difficulty in the final

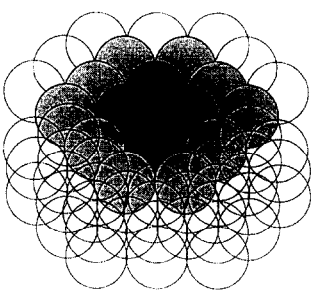

Fig. 1. Cluster geometry and local region of the cluster used to model Ni(111) in the present study. The initial three layer, 62-atom cluster, consists of a surface layer of 28 atoms, a second layer of 17 atoms and a third layer of 17 atoms. The embedding procedure is used to reduce the Ni_{62} cluster to a 28-atom model depicted as shaded atoms: the surface layer of 14 atoms, a second layer of 9 atoms, and a third layer of 5 atoms. All shaded atoms are described by 4s-atomic orbitals; those atoms heavily shaded also contain 3d- and 4p-atomic orbitals. Unshaded atoms are described by neutral atom potentials (see Ref. [34]). All atoms have Phillips–Kleinman projectors $\Sigma|Q_m\rangle\langle Q_m|(-\epsilon_m)$ for the fixed electronic distribution. The positions of the Ni atoms in the cluster model were held fixed with a nearest neighbor Ni–Ni distance of 2.48 Å from the bulk.

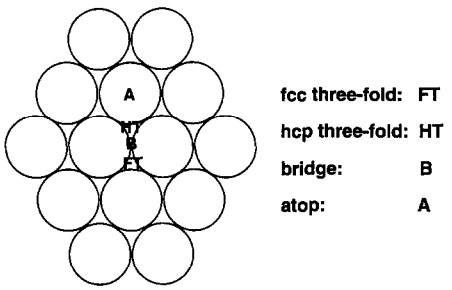

Fig. 2. Adsorption sites: the notation, FT, HT, B, and A, refer to fcc three-fold, hcp three-fold, bridge, and atop Ni sites, respectively. There is second layer Ni atom underneath the hcp three-fold site. Only the first layer of the three-layer cluster is shown.

model is that of a cluster, typically 30 to 40 atoms, in the presence of electrostatic potentials and projectors describing the embedding. Atoms in the surface region and their nearest neighbors do not have effective potentials (except for core electrons). The effective atomic potentials begin at the next shell of atoms and functions are also present in this shell to allow a polarization of the electron distribution near the interface during the course of surface reactions. Details of the procedure are reported in references [33,34]. Fig. 1 shows the cluster geometry and local region of the cluster used to model Ni(111) in the present study. The initial three layer, 62-atom cluster, consists of a surface layer of 28 atoms, a second layer of 17 atoms and a third layer of 17 atoms. The embedding procedure is used to reduce the Ni_{62} cluster to a 28-atom model depicted as shaded atoms: the surface layer of 14 atoms, a second layer of 9 atoms, and a third layer of 5 atoms. All shaded atoms are described by 4s-atomic orbitals; those atoms heavily shaded also contain 3d- and 4p-atomic orbitals. Unshaded atoms are described by neutral atom potentials [34].

The sites considered for C–N containing molecules adsorption on Ni(111) are as follows: a hollow three-fold site with no second layer Ni atom underneath (fcc extension of the lattice); a filled three-fold site with a second layer Ni atom underneath (hcp extension of the lattice); a bridge site and an atop Ni site, denoted by HT, FT, B and A, respectively, as shown in Fig. 2.

The basis orbitals of Ni and H are listed in Ref. [35]. The H basis set includes a double zeta s and p plus a set of 2p functions with an exponent of 0.6. The triple zeta s and p basis for carbon and nitrogen is taken from Whitten [36] and augmented with a set of d polarization functions with an exponent of 0.626 for carbon and 0.913 for nitrogen. Previous studies have shown that these basis orbitals are able to describe the C–N containing molecules [37–39].

3. CN adsorption on Ni(111)

There are three possible types of surface cyanides, namely, η^1-cyanide-C, η^1-cyanide-N, and η^2-cyanide-C,N, bonding to the surface via the C atom, N, and or both the C and N atoms, respectively, as shown in Fig. 3. The η^1-cyanides are the traditionally called end-on bonded CN, and the side-on bonded CN is the η^2-cyanide. Calculated adsorption energies, C- and N-surface equilibrium distances, vibrational frequencies and bond distances for end-on and side-on bonded CN are reported in Table 1. Our calculations showed that CN is able to bind to the surface either via the carbon, or nitrogen, or in a side-on geometry with very small differences in total energy (≈ 2 kcal/mol). Adsorption energies at three-fold, bridge and atop sites are comparable, with the fcc three-fold site more favorable over other adsorption sites by only 2 kcal/mol. At the fcc three-fold site, adsorption energies, relative to the neutral CN radical, are 115, 113, and 113 kcal/mol for η^1-cyanide-N, η^1-cyanide-C, and η^2-cyanide-C,N, respectively. Calculated C–N stretching frequencies

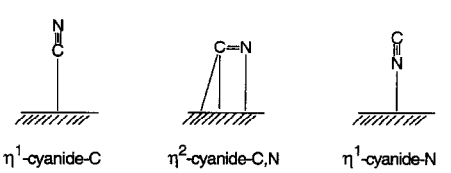

Fig. 3. Possible geometries of surface cyanides, η^1-cyanide-C, η^1-cyanide-N, and η^2-cyanide-C,N, bonding to the metal surface via the C atom, via the N atom, and via both C and N atoms.

Table 1
CN adsorption on Ni(111). Results are for the equilibrium geometry of CN

Site [a]	fcc 3-fold	hcp 3-fold	Bridge	Atop
η^1-cyanide-C				
E_{ads} [b] (kcal/mol)	113	111	113	111
$R_{C-surface}$ [c] (Å)	1.84	1.84	1.88	1.95
R_{C-Ni} [c] (Å)	2.33	2.35	2.25	1.95
C–N stretch (cm^{-1})	1970	1980	1967	1969
C–surface stretch (cm^{-1})	296	306	301	390
η^1-cyanide-N				
E_{ads} [b] (kcal/mol)	115	111	113	109
$R_{N-surface}$ [c] (Å)	1.69	1.72	1.80	1.90
R_{N-Ni} [c] (Å)	2.22	2.24	2.18	1.90
C–N stretch (cm^{-1})	2146	2156	2140	2157
N-surface stretch (cm^{-1})	414	406	501	532
η^2-cyanide-C,N				
E_{ads} [b] (kcal/mol)	113	113	113	113
$R_{ads-surface}$ [c] (Å)	1.96	1.96	1.99	2.03
R_{C-Ni} [c] (Å)	2.42	2.42	2.34	2.03
R_{N-Ni} [c] (Å)	2.33	2.33	2.21	2.34
C–N stretch (cm^{-1})	1845	1850	1840	1870

[a] Fig. 2 shows the adsorption sites. There is a second layer Ni atom underneath the hcp 3-fold site, while there is no second layer Ni atom underneath the fcc 3-fold site.
[b] E_{ads} is relative to CN at infinite separation. Positive values are exothermic. Results are from CI calculations and are corrected for basis superposition effects (3–5 kcal/mol).
[c] $R_{C-surface}$ or $R_{N-surface}$ are the perpendicular distances from carbon or nitrogen to the Ni surface, and R_{C-Ni} and R_{N-Ni} are the corresponding distances from carbon nucleus to the nearest Ni nucleus. C–N bond distance is 1.18 Å for η^1-cyanides and 1.19 Å for the side-on bonded CN, and all are similar to the gaseous value of 1.18 Å.

are 2150, 1970, and 1840 cm^{-1} for η^1-cyanide-N, η^1-cyanide-C, and η^2-cyanide-C,N, respectively.

Fig. 4 shows the variation in CN adsorption energy with respect to β, the angle between the N–C axis and the surface normal. Calculated energy barriers in going from η^1-cyanide-C to η^2-cyanide-C,N, and from η^2-cyanide-C,N to η^1-cyanide-N are very small, ≈ 2 kcal/mol. This indicates that although CN is strongly bound to the surface (at ≈ 115 kcal/mol), within an energy range of ≈ 5 kcal/mol, the molecule is free to rotate to other geometries.

There are a number of other theoretical investigations of CN adsorption on metal surfaces [40–46]. However, terminally bonded CN species were mainly studied. The studies of CN on a Cu(100) surface indicated an electrostatic bond with no preferred molecular orientation [42–46]. Using the atom superposition and electron delocalization molecular orbital (ASED-MO) and cluster model method, Zhou et al. studied CN adsorption on Ni(111) [41]. Although the side-on bonded CN was considered, the end-on bonded CN (through the C atom) configuration was found to be much more preferable than the side-on bonded CN or other configurations. The calculated adsorption energy of the end-on CN was 78 kcal/mol for all the high and low symmetry sites. The side-on CN on Ni(111) was found to be 39 kcal/mol less stable than the end-on geometry [41]. Recent local density functional (LCFTO-LDF) cluster calculations indicated that the CN lies

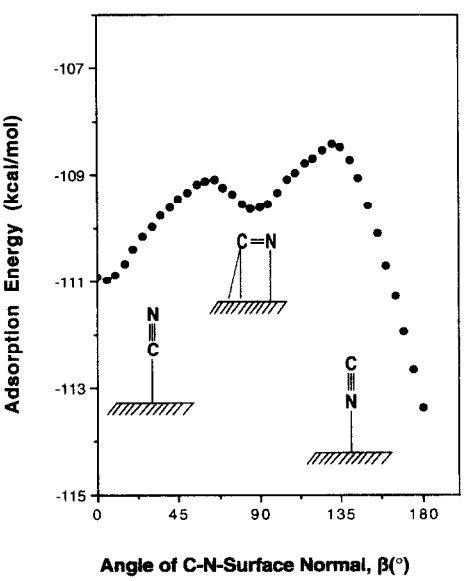

Fig. 4. Adsorption energy (in eV) of CN versus β, the angle between the N–C axis and the surface normal. The left most geometry, corresponding to $\beta = 0°$, is the η^1-cyanide-C, adsorbed at the hcp three-fold site, and the right most geometry, corresponding $\beta = 180°$, is the η^1-cyanide-N, adsorbed in the region between the bridge and fcc three-fold sites. At $\beta = 90°$, the corresponding geometry is the η^2-cyanide-C,N, where the C–N axis is parallel to the substrate.

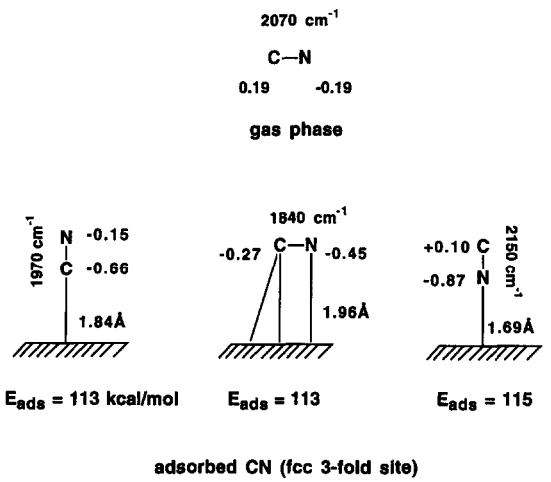

Fig. 5. Adsorption of the end-on and side-on bonded CN on Ni(111). Values of C–N stretching frequency and atomic charge in unit $|e|$ are indicated. The upper results are for gaseous CN. E_{ads} is relative to CN at infinite separation from the surface. Positive values are exothermic.

parallel to the surface with its molecular axis oriented along the [110] azimuthal direction [40]. The LDF calculations, performed on a 8-atom cluster of Ni(110), concluded that the long-bridge site represents best the adsorption geometry for CN on Ni(110). The corresponding adsorption energy was 97 kcal/mol, and the side-on bonded CN was calculated to be the minimum energy geometry. The energy barrier in going from the side-on configuration to the end-on bonded CN was 12 kcal/mol [40]. Our calculated energies are in qualitative agreement with the LDF values.

Fig. 5 summarizes the adsorption properties of CN on Ni(111).

The present calculated adsorption energies of different CN orientations on Ni are relative to gaseous CN at infinite separation. Since the adsorbed CN on the surface resembles CN^-, our results show that the bonding of CN to the Ni surface is still exothermic compared to the free CN^- at infinite separation. Relative to CN^-, the corresponding adsorption energies for η^1-cyanide-N, η^1-cyanide-C, and η^2-cyanide-C,N at the fcc three-fold site are 37, 35, and 35 kcal/mol, respectively.

4. HCN and HNC adsorption on Ni(111)

Calculated adsorption energies, C- and N-surface equilibrium distances, vibrational frequencies and bond distances for end-on bonded HCN and HNC are reported in Table 2. The calculations show that the potential surface is fairly flat for HCN and HNC adsorption. Calculated HCN adsorption energies are 18, 16, 15, and 17 kcal/mol at the fcc three-fold, hcp three-fold, bridge, and atop sites, with the N-surface distances of 2.24, 2.25, 2.28, and 2.06 A, respectively. Calculated HNC adsorption energies are 8.2, 6.5, 8.6, and 11 kcal/mol at the

Table 2
HCN and HNC adsorption on Ni(111). Results are for end-on bonded geometries

Site [a]	fcc 3-fold	hcp 3-fold	Bridge	Atop
HCN				
E_{ads} [b] (kcal/mol)	18	16	15	17
$R_{N-surface}$ [c] (Å)	2.24	2.25	2.28	2.06
R_{N-Ni} [c] (Å)	2.65	2.66	2.60	2.06
ω_{C-N} (cm^{-1})	2220	2225	2215	2200
ω_{C-H} (cm^{-1})	3418	3429	3419	3428
$\omega_{HCN-surface}$ (cm^{-1})	256	266	270	280
r_{C-N} (Å)	1.16	1.16	1.16	1.16
r_{C-H} (Å)	1.07	1.07	1.07	1.07
HNC				
E_{ads} [b] (kcal/mol)	8.2	6.5	8.6	11
$R_{C-surface}$ [c] (Å)	2.08	2.09	2.16	1.92
R_{C-Ni} [c] (Å)	2.52	2.53	2.51	1.92
ω_{C-N} (cm^{-1})	2110	2120	2120	2100
ω_{N-H} (cm^{-1})	3700	3690	3680	3671
$\omega_{HNC-surface}$ (cm^{-1})	250	255	260	280
r_{C-N} (Å)	1.16	1.16	1.16	1.16
r_{N-H} (Å)	1.00	1.00	1.00	1.00

[a] Fig. 2 shows the adsorption sites. There is a second layer Ni atom underneath the hcp 3-fold site, while there is no second layer Ni atom underneath the fcc 3-fold site.

[b] E_{ads} is relative to HCN at infinite separation. In the gaseous ground state, HCN is calculatedto be 14.5 kcal/mol more stable than HNC. Positive values are exothermic. Results are from configuration interaction calculations and are corrected for basis superposition effects (3–5 kcal/mol).

[c] $R_{C-surface}$ or $R_{N-surface}$ are the perpendicular distances from carbon or nitrogen to the Ni surface, and R_{C-Ni} and R_{N-Ni} are the corresponding distances from carbon nucleus to the nearest Ni nucleus.

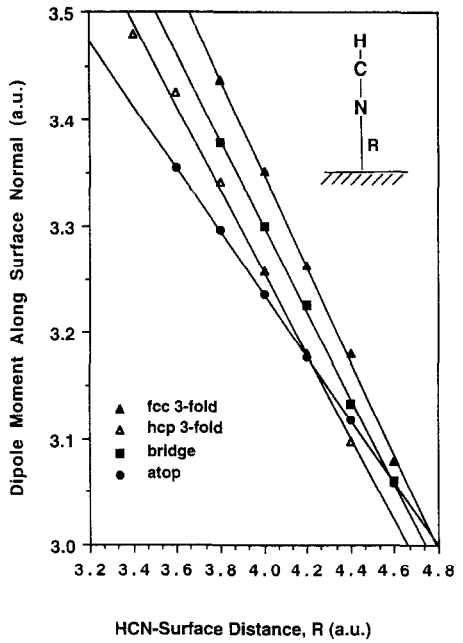

Fig. 6. Calculated dipole moment (1 a.u., 2.54 D) of end-on bonded HCN along the surface normal at various adsorption sites versus the HCN–surface distance. Calculated values of the first derivative of the dipole moment curve, $d\mu/dR$, are -0.44, -0.39, -0.40, and -0.29 for HCN at the fcc three-fold, hcp three-fold, bridge, and atop sites, respectively.

fcc three-fold, hcp three-fold, bridge, and atop sites, respectively. The atop site is the more favorable for the hydrogen isocyanide adsorption, while the fcc three-fold site is favorable for hydrogen cyanide adsorption. The calculated C-surface perpendicular distances are consistently shorter than the N-surface distances for HCN by ≈ 0.15 Å.

Figs. 6 and 7 show the variation in dipole moment along the surface normal with respect to HCN- and HNC–surface distance for the end-on HCN adsorbed at different sites on the Ni(111) surface, respectively. The dipole moment curves are quite similar for HCN at all sites. The values for the first derivative of the dipole moment, $d\mu/dR$, are -0.44, -0.39, -0.40, and -0.29 for HCN at the fcc three-fold, hcp three-fold, bridge, and atop sites, respectively. By this measure, it would appear that HCN at the atop site has the least ionic character. The values of $d\mu/dR$ are -0.06, 0.06, and 0.03 for HNC at the fcc three-fold, hcp three-fold, and bridge sites, respectively. Thus, the slope is ≈ 0. At the bridge and atop sites, the dipole moment curves are nonlinear, indicating relatively stronger covalent bonding.

Comparing both Fig. 6 (for HCN) and Fig. 7 (for HNC), the difference in slopes is large enough to suggest that HNC on the Ni(111) surface has much more covalent character than HCN.

For HCN at the atop site in the equilibrium N-surface distance, the total charge on HCN is $+0.13|e|$, indicating that electrons are transferred to nickel. For HCN adsorbed at high symmetry sites, the net charges on HCN are $-0.06|e|$, $-0.07|e|$ and $-0.09|e|$, at the fcc three-fold, hcp threefold, and bridge sites, respectively. The transferred electrons are mainly localized on the carbon atom. Comparing HCN at the atop and fcc three-fold sites, the net charges on carbon are $+0.07|e|$ and $-0.11|e|$, respectively. It appears that the metal-π back-

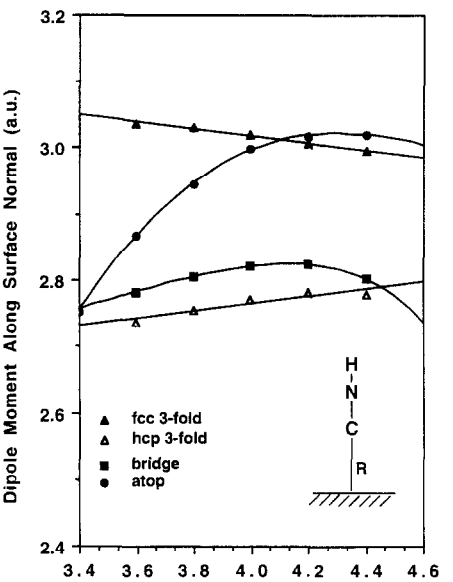

Fig. 7. Calculated dipole moment (1 a.u., 2.54 D) of end-on bonded HNC along the surface normal at various adsorption sites versus the HNC–surface distance. Calculated values of the first derivative of the dipole moment curve, $d\mu/dR$, are -0.06,0.06, and 0.03 for HNC at the fcc three-fold, hcp three-fold, and bridge sites, respectively. For HNC at the atop and bridge sites, the dipole moment curve is no longer linear.

bonding is greater at high symmetry sites than for the atop site. Mulliken populations show very little change in the Ni 3d population; thus, the π back-bonding is accomplished mainly through the 4s orbitals in nearest neighbor atoms defining the high symmetry sites.

The net charges on HNC are $+0.11|e|$ at the atop site, and $+0.04|e|$ at both the three-fold and bridge sites, indicating only a slight electron transfer to the surface. Our calculations show that substantial π back-bonding occurs when HNC is adsorbed causing the nitrogen atom to become more negatively charged. For HNC at the atop site, the π orbitals gain 0.16 electrons compared to the gaseous value, while the Ni 3d orbitals from the Ni atom underneath lose 0.13 electrons compared to the clean surface. This is typical d–π back-bonding, and it causes the net charge on the nitrogen atom to be $-0.41|e|$. In contrast, for the case of N-bonded HCN at the atop site, the π orbitals gained only 0.02 electrons, the net charge on the carbon atom is $+0.07|e|$ and the Ni 3d orbitals from the Ni atom underneath lose only 0.03 electrons. For HNC at the fcc three-fold site, the π orbitals gain 0.12 electrons and the Ni surface loses 0.03 3d electrons from the three neighboring Ni atoms ($0.01|e|$ per Ni atom). In this case, since the net charge on the nitrogen atom is $-0.40|e|$, it appears that the metal-π back-

Table 3
CNH_2 and HCNH adsorption on Ni(111). Results are for equilibrium geometries as shown in Fig. 9

Site [a]	fcc 3-fold	hcp 3-fold	Bridge	Atop	Gas phase
CNH_2					
E_{ads} [b] (kcal/mol)	55.6	55.3	56.5	46.8	—
$R_{C-surface}$ [c] (Å)	1.49	1.50	1.60	2.06	—
R_{C-Ni} [c] (Å)	2.65	2.66	2.02	2.06	—
ω_{C-N} (cm^{-1})	1343	1338	1335	1355	1349
ω_{N-H} (cm^{-1})	3348	3360	3356	3378	3437
$\omega_{C-surface}$ (cm^{-1})	476	486	490	535	—
r_{C-N} (Å)	1.32	1.33	1.32	1.33	1.31
r_{N-H} (Å)	1.02	1.02	1.02	1.02	1.02
∠HNH (degree)	115°	115°	115°	115°	120°
HCNH	Near 3-fold and bridge				Gas phase
E_{ads} [b] (kcal/mol)	88.2				—
$R_{C-surface}$ [c] (Å)	1.88				—
$R_{N-surface}$ [c] (Å)	1.88				—
ω_{C-N} (cm^{-1})	1457				1850
ω_{N-H} (cm^{-1})	3349				3345
ω_{C-H} (cm^{-1})	2935				2954
r_{C-N} (Å)	1.32				1.22
r_{N-H} (Å)	1.03				1.03
r_{C-H} (Å)	1.11				1.11
∠HNC (degree)	120°				120°
∠HCN (degree)	110°				130°

[a] Fig. 2 shows the adsorption sites. There is a second layer Ni atom underneath the hcp 3-fold site, while there is no second layer Ni atom underneath the fcc 3-fold site.

[b] E_{ads} is relative to CNH_2 at infinite separation from the surface and positive values are exothermic. In gas phase, HCNH is about 15 kcal/mol more stable than CNH_2. Results are from configuration interaction calculations and are corrected for basis superposition effects (4–5 kcal/mol).

[c] $R_{C-surface}$ or $R_{N-surface}$ are the perpendicular distances from carbon or nitrogen to the Ni surface, and R_{C-Ni} and R_{N-Ni} are the corresponding distances from carbon nucleus to the nearest Ni nucleus.

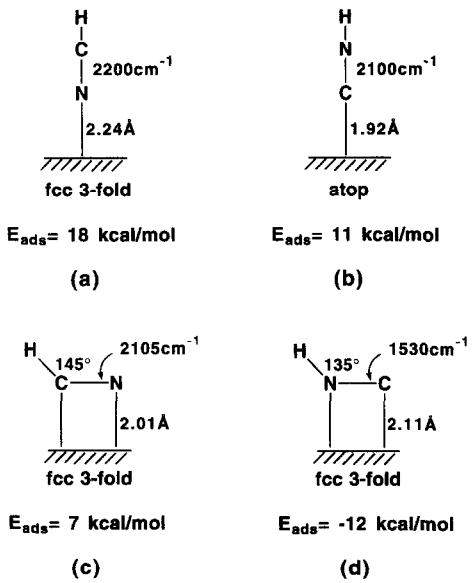

Fig. 8. Calculated equilibrium geometries for end-on and side-on bonded HCN and HNC on Ni(111), respectively. E_{ads} is relative to HCN at infinite separation from the surface and positive values are exothermic. The side-on bonded HNC species is found unbound by 12 kcal/mol. In the gas phase the ground state of HNC is calculated to be 14.5 kcal/mol higher in energy than HCN.

bonding at the three-fold site is accomplished mainly through the Ni 4s orbitals.

Other HCN and HNC adsorption geometries on nickel have also been calculated [38]. Tilting either the H atom or H–C bond or N–H bond away from the surface normal destabilizes the chemisorption system. The side-on bonded HCN and HNC with the C–N bond parallel to the substrate are energetically less stable than the corresponding end-on bonded species.

Fig. 8 summarizes the adsorption properties of HCN and HNC on Ni(111).

5. CNH_2 and HCNH adsorption on Ni(111)

Table 3 reports the calculated adsorption energies, C- and N-surface equilibrium distances, vibrational frequencies, bond distances and bond angles, and Fig. 9 depicts the calculated adsorption geometry of CNH_2 and HCNH on the Ni(111) surface. For CNH_2 adsorption, the calculated adsorption energies are 55.6, 55.3, 56.5, and 46.8 kcal/mol at the fcc three-fold, hcp three-fold, bridge, and atop sites, respectively, with respect to CNH_2 at infinite separation. The bridge site is the most stable adsorption site with a C-surface distance of 1.60 Å (corresponding to the C to the nearest Ni distances of 2.02 Å). The plane of the CNH_2 molecule is nearly perpendicular to the substrate. Tilting the plane of NH_2 away from the surface normal by 10°, 20°, and 30°, the energy slightly increases by +0.2, +1.2, and +3.5 kcal/mol. In general, the calculated bond distances of C–N and N–H, the ∠HNH angle, and the vibrational frequencies of C–N and N–H are very similar to the gaseous values.

It should be pointed out that since the difference of calculated adsorption energy for CNH_2 between the bridge and three-fold sites is quite small (≈ 1 kcal/mol), adsorbate–adsorbate in-

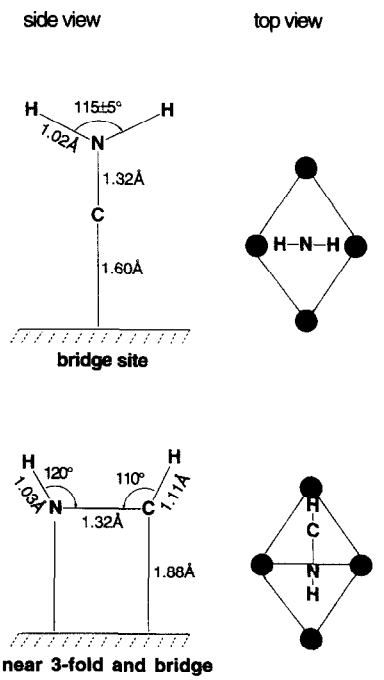

Fig. 9. Side view and top view for adsorbed CNH_2 and HCNH on Ni(111). Adsorbed HCNH is energetically more stable than CNH_2 by 31.7 kcal/mol. Both CNH_2 and HCNH are planar geometries on the surface.

teractions could overcome this small differences. Thus, CNH_2 is able to adsorb at both sites.

Our calculated vibrational frequencies of $\omega_{CN} = 1335$ cm^{-1} and $\omega_{NH} = 3356$ cm^{-1} for CNH_2 on Ni(111) are in good agreement with the FT-IRAS values of 1323 cm^{-1} and 3363 cm^{-1} for observed on the Pt(111) surface [47,48] and are somewhat different from the HREELS values for CNH_2 on the Ru(001) surface. The observed C–N and N–H stretching frequencies on Ru(001) are 1620 cm^{-1} and 3250 cm^{-1}, and the adsorbed CNH_2 is determined to be bonded at a μ-bridging site [49]. Thus, the behavior of adsorbed CNH_2 on Ru(001) is different than on Ni(111) and Pt(111).

For HCNH adsorbed on Ni(111), we found that the most stable geometries are for the C–N bond parallel to the surface at all the adsorption sites investigated. The energy minimum occurs when the midpoint of the C–N bond is above a hollow three-fold, as shown in Fig. 9. The corresponding adsorption energy is 88.2 kcal/mol with respect to CNH_2 at infinite separation. The present calculations indicate that HCNH is energetically more stable than CNH_2 on Ni(111) by about 31.7 kcal/mol. Moving HCNH to the vicinity of three-fold and bridge sites shows little energy change (≈ 1 kcal/mol).

The calculated vibrational frequencies of HCNH on Ni(111) are $\omega_{CN} = 1457$ cm^{-1}, $\omega_{CH} = 2935$ cm^{-1}, and $\omega_{NH} = 3349$ cm^{-1}. Compared to the calculated gaseous values, the C–N stretching frequency decreases 400 cm^{-1}. The ~ 400 cm^{-1} redshift indicates a strong metal-π back-bonding. This is consistent with the longer C–N bond length on the surface (1.32 Å versus 1.22 Å). These results suggest that both C and N atoms are involved in bonding with the surface. Thus, chemisorbed HCNH on the Ni(111) surface is characterized as η^2-HCNH.

Based upon the present calculated vibrational frequencies, we would suggest that the infrared bands at 3371, 1565, and 1325 cm^{-1}, observed by Erley and Hemminger using IRAS from the decomposition of methylamine on Pt(111) surface, may belong to adsorbed CNH_2, not to adsorbed HCNH [50]. The bands at 3371 and 1325 cm^{-1} may correspond to the NH stretching and the CN stretching, respectively.

The calculated present geometry for HCNH is in good agreement with the proposed structure of μ_3—η^2—HCNH on Ru(001) [49]. The observed stretching frequencies are 1450 cm^{-1} for C–N, 2920 cm^{-1} for C–H, and 3250 cm^{-1} for N–H, respectively.

The present results are also in an agreement with the studies of HCNH on the carbon covered W(001) surface [51,52]. HREELS studies by Serafin and Friend gave the C–N stretching, C–H stretching, and N–H stretching bands at 1400, 2940, and 3360 cm^{-1}, which are in good agreement with our calculated values. The determined C–N bond distance by NEXAFS is 1.34 ± 0.04 Å, in excellent agreement with the present calculation of 1.32 Å. The proposed geometry for HCNH is that the C–N bond vector is inclined at an angle of $58° \pm 10°$ with respect to the surface normal. In the present calculations, we found that tilting the C–N bond away from the parallel position destabilizes the system. If all the bond angles and bond distances of HCNH are kept stationary, tilting the N atom away from the parallel position by 10°, 20°, and 30° increases the energy about 3, 12, and 18 kcal/mol, respectively. The tilted HCNH corresponds to the C–N bond vector away from the surface normal by 80°, 70°, and 60°, respectively. Thus, our studies strongly suggest that the C–N bond of adsorbed HCNH is nearly parallel to the Ni(111) surface.

The present theoretical calculations show that the molecular structure of HCNH is greatly perturbed upon adsorbed on the Ni(111) surface. In contrast, the bonding between CNH_2 and the surface has little effect on the molecular structure of CNH_2.

If we take hydrogen adsorption energy as 63 kcal/mol on nickel, our calculations would predict:

1. Reaction CNH_2 (ads) → HNC (ads) + H (ads) is 22 kcal/mol exothermic.

2. Reaction HCNH (ads) → HNC (ads) + H (ads) is 2 kcal/mol endothermic.
3. Reaction HCNH (ads) → HCN (ads) + H (ads) is 5 kcal/mol exothermic.
4. Reaction HNC (ads) → CN (ads) + H (ads) is 30 kcal/mol exothermic.
5. Reaction HCN (ads) → CN (ads) + H (ads) is 21 kcal/mol exothermic.

6. Summary

A many-electron embedding approach for treating chemisorption and surface reactions on metal surfaces at an ab initio configuration interaction level is briefly described. Adsorption of CN, HCN, HNC, CNH_2 and HCNH molecules on Ni(111) are reported. The Ni(111) surface is modeled as a three-layer, 28-atom cluster with the Ni atoms fixed at the bulk distances. The present calculations show that CN is able to bind to the surface either via the C, or N, or in a side-on geometry with very small differences in total energy (≈ 2 kcal/mol). Adsorption energies at 3-fold, bridge and atop sites are comparable, $113 \sim 115$ kcal/mol, with the fcc 3-fold site more favorable over other adsorption sites by ≈ 2 kcal/mol. Calculated C–N stretching frequencies are 2150, 1970, and 1840 cm^{-1} for end-on N-bonded, end-on C-bonded, and side-on bonded CN, respectively. Within an energy range of ≈ 5 kcal/mol, the CN molecule is free to rotate to other geometries. Both HCN and HNC bind to the surface in an end-on geometry with the molecular axis perpendicular to the surface. The calculated adsorption energy for the end-on HCN is 18 kcal/mol, and 11 kcal/mol for the end-on HNC. The side-on bonded HCN and HNC with the C–N bond parallel to the surface are energetically less stable than the corresponding end-on bonded species. Both CNH2 and HCNH strongly bind to the surface with HCNH more stable by 32 kcal/mol. CNH_2 is adsorbed at a bridge site via the C atom. Both C and N atoms in HCNH are involved in bonding to the surface with the C–N bond parallel to the surface.

Acknowledgements

Support of the work by the U S. Department of Energy is gratefully acknowledged. I would like to thank Dr. J.L. Whitten for helpful discussions.

References

[1] G. Pacchioni, P.S. Bagus and F. Parmigiani (Eds.), Cluster Models for Surface and Bulk Phenomena, NATO ASI Series, Vol. 283 (Plenum Press, New York 1992).
[2] E. Shustorovich (Ed.), Metal–Surface Reaction Energetics: Theory and Applications to Heterogeneous Catalysis, Chemisorption and Surface Diffusion (VCH Publishers, New York 1991).
[3] R.A. van Santen, Theoretical Heterogeneous Catalysis (World Scientific, Singapore 1991).
[4] D.R. Salahub and N. Russo (Eds.), Quantum Chemical Models of Chemisorption on Metal Surfaces, NATO ASI Series, Vol. 378 (Kluwer Academic, Dordrecht, The Netherlands, 1992).
[5] D.R. Salahub and M.C. Zerner (Eds.), The Challenge of d and f Electrons: Theory and Computation, ACS Symposium Series, Vol. 394 (ACS, Washington, 1989).
[6] C.W. Bauschlicher, Jr., H. Partridge, J.A. Sheehy, S.R. Langhoff and M. Rosi, J. Phys. Chem. 96 (1992) 6969.
[7] G. Pacchioni and P.S. Bagus, Chem. Phys. 177 (1993) 373.
[8] P.S. Bagus and F. Illas, Phys. Rev. B 42 (1990) 10852.
[9] J.M. Ricart, A. Clotet, F. Illas and J. Rubio, J. Chem. Phys. 100 (1994) 1988.
[10] P.S. Bagus and G. Pacchioni, J. Chem. Phys. 102 (1995) 879.
[11] I. Panas, J. Schule and P.E.M. Siegbahn, Chem. Phys. Lett. 149 (1988) 265; J. Schule, P. Siegbahn and U. Wahlgren, J. Chem. Phys. 89 (1988) 6982; I. Panas and P.E.M. Siegbahn, J. Chem. Phys. 92 (1990) 4625.
[12] U. Wahlgren and P. Siegbahn, in: D.R. Salahub and N. Russo (Eds.), Metal–Ligand Interactions: From Atoms, to Clusters, to Surfaces, NATO ASI Series, Vol. 378 (Kluwer Academic, Dordrecht, The Netherlands, 1992).
[13] O. Swang, K. Faegri, Jr., O. Gropen, U. Wahlgren and P. Siegbahn, Chem. Phys. 156 (1991) 379.
[14] L. Triguero, U. Wahlgren, P. Boussard and P. Siegbahn, Chem. Phys. Lett. 237 (1995) 550.
[15] E.J. Baerends, in: G. Pacchiohi, P.S. Bagus and F. Parmigiani (Eds.), Cluster Models for Surface and Bulk Phenomena, NATO ASI Series, Vol. 283 (Plenum Press, New York 1992) p. 189.
[16] H. Sellers, Chem. Phys. Lett. 178 (1991) 351.

[17] H. Sellers, Surf. Sci. 264 (1992) 177; 294 (1993) 99.
[18] H. Sellers, A. Ulman, Y. Shnidman and J.E. Eilers, J. Am. Chem. Soc. 115 (1993) 9389.
[19] C. Pisani, J. Mol. Catal. 82 (1993) 229.
[20] S. Cassassa and C. Pisani, Phys. Rev. B 51 (1995) 7805.
[21] S. Crampin, J.B.A.N. van Hoof, M. Nekovee and J.E. Inglesfield, J. Phys. Condens. Matter 4 (1992) 1475.
[22] W. Guerts and F.M.M. Ravenek, J. Chem. Phys. 84 (1986) 1613.
[23] Y. Fukunishi and H. Nakatsuji, J. Chem. Phys. 97 (1992) 6535.
[24] R. Wu, A.J. Freeman and G.B. Olson, Phys. Rev. B 47 (1993) 6855, and references therein.
[25] B. Weimert, J. Noffke and L. Fritsche, Surf. Sci. 264 (1992) 365.
[26] G. te Velde and E. Baerends, Chem. Phys. 177 (1993) 399.
[27] P.J. Feibelman, Annu. Rev. Phys. Chem. 40 (1989) 261; Phys. Rev. Lett. 69 (1992) 1568, and references therein.
[28] C. Dykstra and B. Kirtman, Annu. Rev. Phys. Chem. 41 (1990) 155.
[29] B. Hammer, K.W. Jacobsen and J.K. Nørskov, Phys. Rev. Lett. 69 (1992) 1971.
[30] S. Krüger and N. Rösch, J. Phys. Condens. Matter 6 (1994) 8149.
[31] J.D. Head and S.J. Silva, Int. J. Quant. Chem. Symp. 26 (1992) 229.
[32] J.D. Head and S.J. Silva, J. Chem. Phys. 104 (1996) 3244.
[33] J.L. Whitten, Chem. Phys. 177 (1993) 387.
[34] J.L. Whitten and H. Yang, Int. J. Quant. Chem. Symp. 29 (1995) 41.
[35] H. Yang and J.L. Whitten, J. Chem. Phys. 89 (1988) 5329.
[36] J.L. Whitten, J. Chem. Phys. 44 (1966) 359.
[37] H. Yang, T.C. Caves and J.L. Whitten, J. Chem. Phys. 103 (1995) 8756.
[38] H. Yang and J.L. Whitten, J. Phys. Chem. 100 (1996) 5090.
[39] H. Yang and J.L. Whitten, Chem. Phys. Lett. 251 (1996) 20.
[40] M.G. Ramsey, D. Steinmuller, F.P. Netzer, S. Kostlmeier, J. Lauber and N. Rosch, Surf. Sci. 307–309 (1994) 82.
[41] X.-Y. Zhou, D.-H. Shi and P.-L. Cao, Surf. Sci. 223 (1989) 393.
[42] P.B. Bagus, C.J. Nelin, W. Muller, M.P. Philpott and H. Seki, Phys. Rev. Lett. 58 (1987) 559.
[43] K. Hermann, W. Muller and P.B. Bagus, J. Electron. Spectrosc. Relat. Phenom. 39 (1986) 107.
[44] M.P. Philpott, P.B. Bagus, C.J. Nelin and H. Seki, J. Electron. Spectrosc. Relat. Phenom. 45 (1987) 169.
[45] C.J. Nelin, P.B. Bagus and M.P. Philpott, J. Chem. Phys. 87 (1987) 2170.
[46] P.B. Bagus, C.J. Nelin, K. Hermann and M.P. Philpott, Phys. Rev. B. 36 (1987) 8169.
[47] D. Jentz, H. Celio, P. Mills and M. Trenary, Surf. Sci. 341 (1995) 1.
[48] D. Jentz, M. Trenary, X.D. Peng and P. Stair, Surf. Sci. 341 (1995) 282.
[49] D.F. Johnson, Y. Wang, J.E. Parmeter, M.M. Hills and W.H. Weinberg, J. Am. Chem. Soc. 114 (1992) 4279.
[50] W. Erley and J.C. Hemminger, Surf. Sci. 316 (1994) L1025.
[51] J.G. Serafin and C.M. Friend, J. Phys. Chem. 92 (1988) 6694.
[52] P.A. Stevens, R.J. Madix and C.M. Friend, Surf. Sci. 205 (1988) 187.